Probe field enhancement in photonic crystals by upconversion nanoparticles

Jingyu Zhang,[a] Teresa E. Pick, Daniel Gargas, Scott Dhuey, Emory M. Chan, Ying Wu, Xiaogan Liang, P. James Schuck, Deirdre L. Olynick, Brett A. Helms, and Stefano Cabrini[b]
Molecular Foundry, Lawrence Berkeley National Laboratory, 1 Cyclotron Rd, Berkeley, California 94720

(Received 27 July 2011; accepted 26 October 2011; published 18 November 2011)

Lanthanide-doped upconverting nanoparticles, converting low frequency light to high frequency light through a multiphoton process, have shown interesting properties for bioimaging. Here, the authors describe a method to deposit a thin layer of upconverting Er^{3+} doped $NaYF_4$ nanoparticles (15 to 25-nm) on a quasi-zero-average-index crystal over a 2×4 mm area to observe light propagation through the structure. Assisted by the photoluminescence of the nanoparticles with upconverting three-photon process, the enhanced field intensity confined in photonic crystals at near infrared wavelength is detected in visible green light under conventional optical microscope. This new technique has distinct advantages over the typical near infrared setups with infrared camera or near-field scanning optical microscope setups. © *2011 American Vacuum Society*.
[DOI: 10.1116/1.3662086]

I. INTRODUCTION AND MOTIVATION

Photonic crystals have the ability to confine and manipulate light and are playing a major role in the rapid development of today's information and communication technology.[1,2] Here, we propose a new technique to map propagation and confinement of near infrared (NIR) light in photonic crystals (PC) based on the use of upconverting nanoparticles (UCNPs). Er^{3+} doped $NaYF_4$ nanoparticles deposited on the open surface of the PC convert 1.55 μm light to visible wavelengths through multiphoton absorption based on sequential energy transfers involving real metastable-excited states.[3,4] This new technique has distinct advantages over the typical NIR setups composed by micro-nanostage and IR camera[5,6] with resolution limitation due to the NIR wavelength, or near-field scanning optical microscope setups which are limited by extremely shallow depth of field and long scanning times. The upconversion method has a three-fold increase in resolution due to detection of green instead of IR wavelengths. The upconversion luminescence (UCL) of the 550 nm Er^{3+}:$^4S_{3/2} \rightarrow {}^4I_{15/2}$ transition monotonically increases with increasing fluences (at NIR) for a very large range of intensity. The photoluminescence (PL) intensity reflects the relative strength of local field intensity on PC. When the input intensity is low (<1 W/cm^2), the three-photon process for emission of visible light is proportional to the cube of the 1.55 μm excitation intensity ($I_{PL} \propto I_{\omega}^3$).[7–9] The PL image is much sharper than the corresponding IR image at low input intensity for a Gaussian laser beam distribution. At a higher intensity ($\sim$500 W/cm^2), the UCL in the visible spectrum is close to a linear response of the input NIR intensity ($I_{PL} \propto I_{\omega}$) due to the saturation effects in the intermediate energy states,[9] allowing UCL to remain effective for imaging field enhancement detection at high fluences. The intensity of the PL at one visible wavelength (550 nm) is the unit area of PL power integrated with all nanoparticles. Therefore, to extract precise NIR field strengths from upconversion intensity maps, the upconverting nanoparticles must be deposited uniformly in the photonic crystals over a very large area. In this paper, we present a facile approach to deposit a uniform, thin layer of nanoparticles on PC surfaces over large areas, enabling the detection of localized electrical field intensity differences with optical microscopy.

Previously, we introduced a quasi-zero-average-index (QZAI) photonic crystals composed of negative index ($n=-1$) PC and positive index ($n=1$) air in periodic arrays.[5] This structure allows focusing of 1.55 μm wavelength light in a Si waveguide under transverse mode (TM) polarized excitation. This structure will be exploited and deposited by UCNPs for image testing. We discuss high aspect ratio Si PC fabrication, nanoparticle synthesis and the deposition of a thin layer of nanoparticles over the large area PC surface. The nanoparticle deposition process was optimized for high uniformity as a key for signal interpretation. The schematic of fabrication flows has been shown in Fig. 1. Via these films, we detect the 550 nm PL signal emitted from the nanoparticles which arises due to the upconversion of the propagating NIR field intensity in the PC.

II. PHOTONIC CRYSTALS FABRICATION

We fabricate a 2×4 mm structure composed of negative index ($n=-1$) PC on silicon and positive index ($n=1$) air slabs, arranged in a periodic 1D array. A 1.55 μm wavelength light with TM polarization, entering parallel to the plane of the silicon surface and perpendicular to the length of the stripe, is focused by the PC and the air stripe due to light bending at the interface of positive and negative index structures. In the previous work,[5] the PC structure was etched into silicon using a gas chopping plasma etching process which alternates an etching step using SF_6, Ar with a passivation step using CHF_3 and CH_4. One cycle consists of

[a]Electronic mail: jyzhang@lbl.gov
[b]Electronic mail: scabrini@lbl.gov

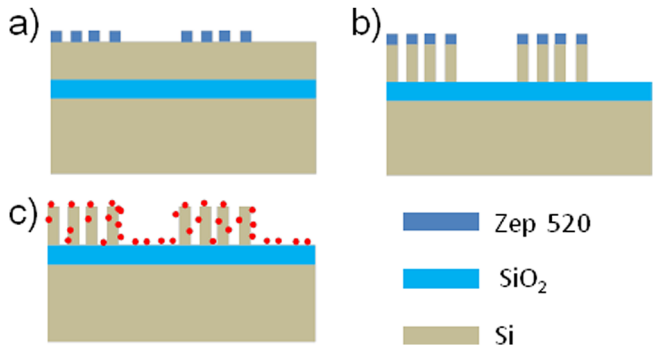

FIG. 1. (Color online) Fabrication of the UCNP deposited QZAI structure: (a) E-beam lithography, (b) Si plasma etching at cryogenic temperatures, and (c) nanoparticle deposition.

one step of etching and passivation and the overall process requires hundreds of cycles for the deep etching (~1.5 to 2 μm) of the high aspect ratio features (~10) which compose the PC. There are several disadvantages for gas chopping plasma etching. In our system, the overhead required to switch between the steps make the etching process slow. The etch rates are ~1 μm/hour. In addition, the process causes major serious chamber contamination due to passivant deposition throughout the chamber. Finally, the alternating step process results in a characteristic sidewall ripple of 10–100 nm. The roughness can increase the loss for photonic devices.[10] Here we optimize an improved etching process which uses SF_6/O_2 plasma chemistry at cryogenic wafer temperatures.[11,12] Starting with a silicon-on-insulator (SOI) wafer (1.5 μm silicon layer on top of 1 μm oxide layer), we spin on ZEP 520, a positive electron beam (EB) resist at a thickness of 370 nm. The resist is patterned using a Vistec VB300UHR EWF electron-beam lithography (EBL) System, and developed with n-amyl acetate. The EB patterned resist is used as a mask to etch the underlying silicon layer, down to the SOI, in an Oxford Plasmalab 100 ICP/RIE with resist mask. The SF_6 chemistry provides the free radicals for isotropic Si etching, while O_2 promotes the growth (at cryogenic temperatures) of a passivation film. This passivation film, with a generic temperature sensitive formula $Si_xF_yO_z$, protects the side walls of the etched structures and disappears after warming to room temperature leaving behind a clean surface.[13,14] Here, the etching was performed at −120 °C. The etch program steps include 1) wafer cool down (2 min), 2) plasma strike (RF power 100 W, ICP power 700 W, SF_6 42 sccm and O_2 15 sccm, 7 mTorr chamber pressure, 3 sec); 3) O_2 passivation (RF power 100 W, ICP power 700 W, SF_6 42 sccm and O_2 15 sccm, 7 mTorr chamber pressure, 6 sec); 4) main etch (RF power 100 W, ICP power 700 W, SF_6 42 sccm and O_2 7 sccm, etching time 70 sec). In the main etch step, we examined the SF_6/O_2 gas flow ratio given that slight changes in oxygen flow produce significant effects on the overall etch features.[11] The sidewall slope can be varied from positive to negative and with sufficient precision that completely vertical side walls can be obtained over micros in height. The overall profile changes from negative to positive as this ratio is decreased as there is a delicate balance between passivation and etching. Low frequency power (2 W, 5k Hz, pulsed on and off with a duty cycle 50%) was added at the lower electrode to decrease notching at the sidewalls due to ion deflection due to charging. A high aspect ratio with critical dimension of 100-nm and 1500-nm etching depth is achieved with a sidewall slope of 90°. The ICP etching results are shown in Fig. 2. The sample is then cleaned by RCA1 (NH_4OH: H_2O_2:H_2O =1:1:5) and RCA3 (HCl: H_2O_2: H_2O=1:1:6) at 80 °C to remove organic and metallic contaminants for nanoparticles deposition.

III. NANOPARTICLE SYNTHESIS

The β-$NaYF_4$: 10% Er^{3+} nanoparticles were synthesized using a modification of a recently reported procedure.[15,16] Oleic acid was used as the surfactant, to control the size and shape of the $NaYF_4$: Er^{3+} nanoparticles, which showed different shapes when the concentration of oleic acid was changed. Nanoparticles were drop-cast from a hexane dispersion and characterized by SEM, *x* ray diffraction (XRD) and PL spectroscopy. A SEM image of the nanoparticles deposited via drop-casting is shown in Fig. 3(a). The average diameter of the nanoparticles was determined to be 20 nm

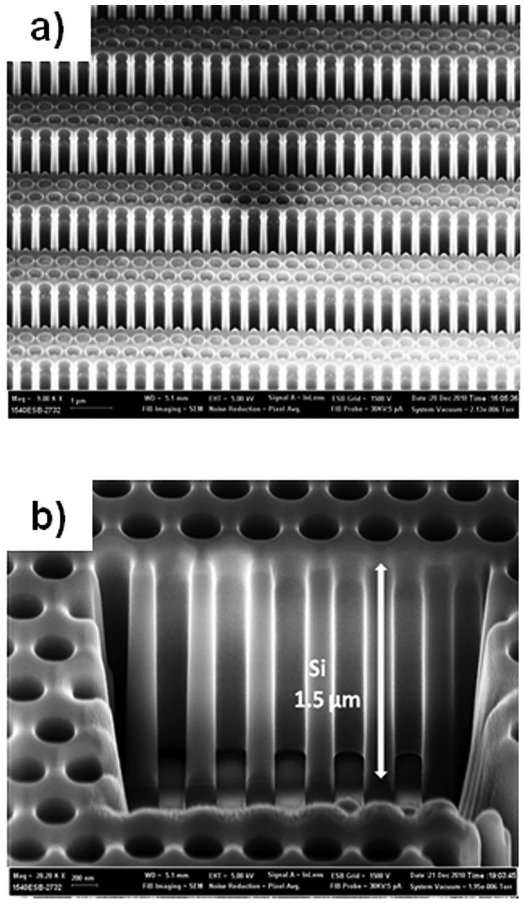

FIG. 2. Scanning electron microscope (SEM) pictures of (a) the etched QZAI at a 45° angle, (b) the inside of the etched PC hole arrays at a 54° angle revealed after focused ion beam (FIB) etching. The air hole radius is 180 nm and pitch (p) between neighboring holes center is 472 nm. The PC slab width is $(3\sqrt{3}/2 + 0.4)p$ and the grating pitch is $3\sqrt{3}p$.

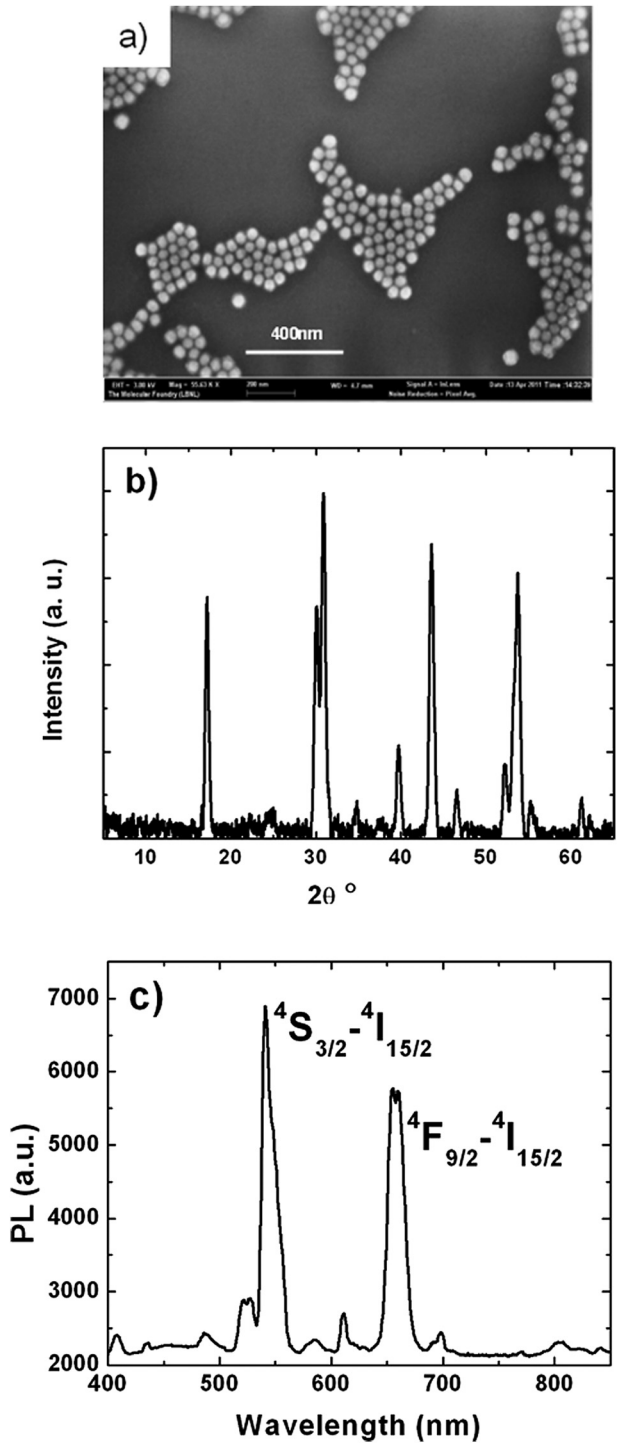

FIG. 3. Characterization of the 10 % Er^{3+} doped β-$NaYF_4$:Er nanoparticles, (a) SEM image, (b) Powder X-ray diffraction (XRD) pattern, and c) PL spectrum with 1550 nm CW laser excitation (Power density = 500 W/cm^2). The green emission at 550 nm and red emission at 670 nm indicate the Er energy transitions from $^4S_{3/2}$ to $^4I_{15/2}$ and $^4F_{9/2}$ to $^4I_{15/2}$, respectively.[17]

with a range of ±5 nm. The nanoparticle samples were characterized by XRD utilizing a Bruker D8-Discover x-ray diffractometer. Samples were drop-cast onto thin glass cover slips from hexanes and allowed to dry. The XRD pattern [Fig. 3(b)] shows that pure β-$NaYF_4$ nanoparticles were obtained and the peaks match well with the standard spectral lines of β-$NaYF_4$ [JCPDS #(01-077-0936)]. The PL spectrum of the Er^{3+} doped nanoparticles with 1.55 μm CW diode laser (Power density = 500 W/cm^2) excitation are shown in Fig. 3(c). The emission bands can be assigned to transitions within the 4*f* manifolds of the Er^{3+} ions. The strongest two emission bands, green emissions at 550 nm and red emission at 670 nm is due to transitions from the $^4S_{3/2}$ to $^4I_{15/2}$ and $^4F_{9/2}$ to $^4I_{15/2}$ manifolds,[17] respectively. The Er^{3+} doped $NaYF_4$ nanoparticles with visible emission under NIR excitation will probe field enhancement at NIR in the QZAI photonic crystal.

IV. NANOPARTICLE DEPOSITION ON PHOTONIC CRYSTAL

For deposition of the nanoparticles, the surface properties of both the nanoparticles and that Si PC are critical. Nonpolar hydrophobic molecules prefer other hydrophobic molecules and nonpolar solvents whereas hydrophilic molecules have a tendency to cling to other hydrophilic molecules. During the synthesis process, β-$NaYF_4$ nanoparticles are ultimately passivated with hydrophobic oleate ligands and dispersed in hexanes to form colloidal solutions with hydrophobic properties.

For surface compatibility with the oleate terminated nanopartices, we treat the Si PC with a hydrophobic layer. A fluoroakylsilane (FAS) in particular, *1H*, *1H*, *2H*, *2H*-perfluorodecyltri-chlorosilane ($CF_3(CF_2)_7(CH_2)_2SiCl_3$), is applied to the Si PC to create a hydrophobic surface.[18] FAS is deposited at a temperature 90 °C for 10 min – 1 h. Contact angle measurements after 10 min give a water contact angle of 110°. After FAS treatment of the PC, the nanoparticles are deposited. The PC sample is placed in a beaker containing the particle dispersion in hexanes with silicon substrate lean against the beaker sidewall with the PC trenches perpendicular to the beaker bottom. We leave the sample evaporating (2–3 h) in a ventilation hood until the solution dries leaving the nanoparticles behind. Figure 4 shows SEM images of nanoparticles deposited on the PC crystal. We observe a layer of nanoparticles covering the PC structure over the entire 2- × 4-mm area. The SEM picture of sample is shown in Fig. 4(a). The images with large magnification are shown in Figs. 4(b), 4(c) and 4(d). Particles are not only visible on the open side walls, but also in the interior walls of small holes and on the unpatterned SiO_2 areas. At the bottom of the vertical sections of the PC as shown in Fig. 4(c) and 4(d), particles were not always deposited. We attribute this to inefficient FAS coverage on the surface as increasing the FAS deposition time to 1 h promoted the coverage of particles over the entire vertical PC features.

V. CHARACTERIZATION

To evaluate the functionality of the upconverting nanoparticles as probe for NIR light, we compare green light UCL images of the QZAI device and adjacent plain silicon grating both decorated with the nanoparticles. The experimental setup is schematically illustrated in Fig. 5(a). The QZAI device is illuminated with a continuous wave (CW) laser at 1550 nm wavelength. The laser spot is focused on

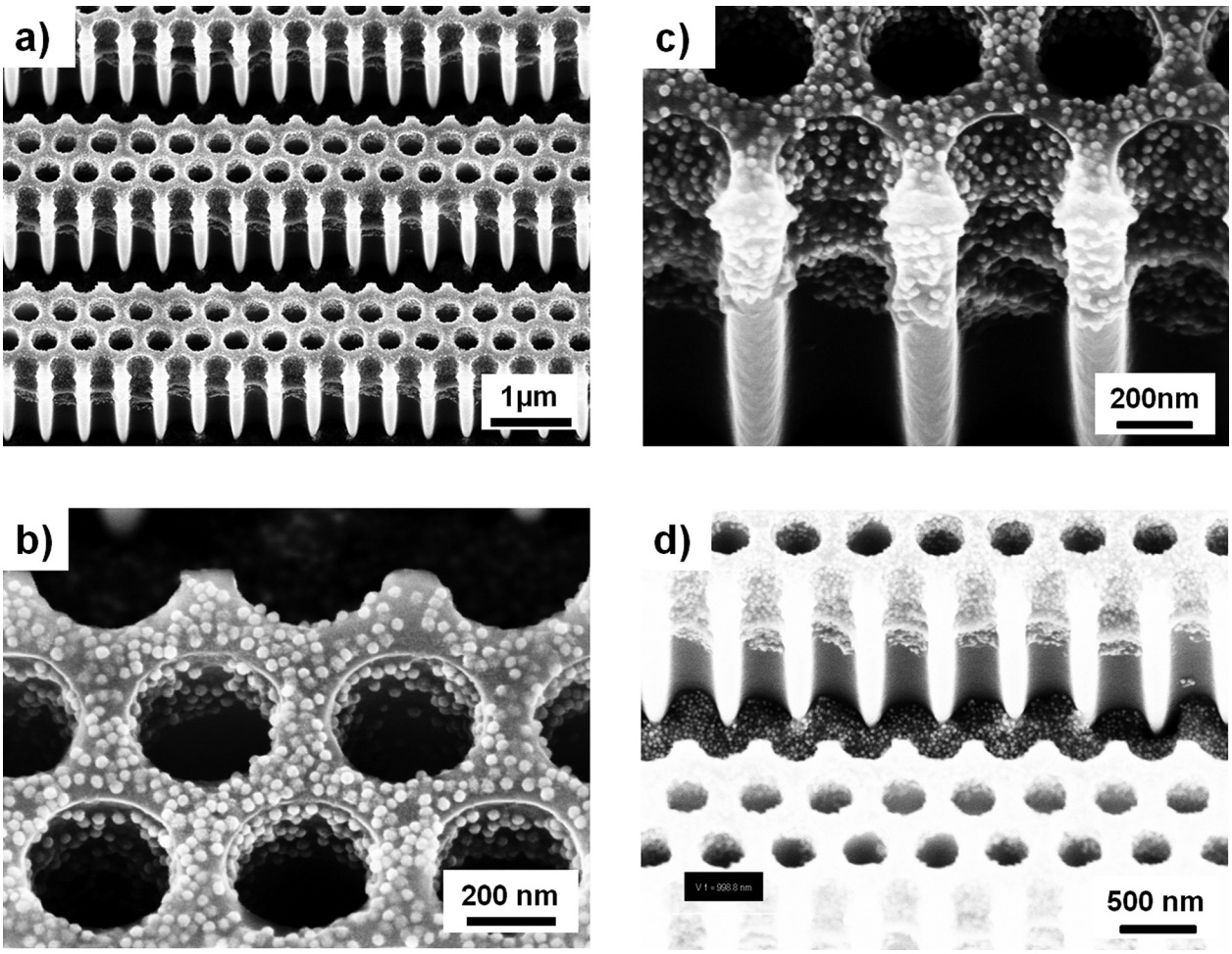

FIG. 4. SEM characterization of nanoparticle deposition (a) on FAS treated PC structure; (b) on the wall of small holes, (c) on the open side walls, and (d) on the SiO_2 surface below the air slab.

the top surface of the sample with $\theta = 30°$ vertical angle so part of the beam can be coupled into the photonic structure. The green PL signal from the nanoparticles was collected by 0.4 numerical aperture (NA) objective with a monochromator and routed to a CCD camera sensitive to the 550 nm Er^{3+}:$^4S_{3/2} \rightarrow {}^4I_{15/2}$ emission. The UCL spectrum is collected with 30 sec exposures at 1550 nm excitation with power density 500 W/cm^2. Also noted in Fig. 5(a) the relevant axes are: the x direction is parallel to the plane of the substrate but perpendicular to the grating formed by the QZAI device, the y direction is perpendicular to the plane of the substrate, and the z direction is parallel to both the plane of the substrate and the grating structure.

In Ref. 5, the field propagating inside the QZAI PC is simulated using a FDTD code. The intensity of the electric field component E_y (TM polarization) is enhanced at the self-focused image spots and propagates along the x direction. The light propagating in z direction (E_z) does not possess the same effect of auto collimation and dissipates. Therefore, the E_y field intensity (and so the PL signal from the nanoparticles) differs when laser is incident either perpendicular or parallel to the QZAI one dimensional (1D) grating direction. So, both incident light directions were tested. Figure 5(b) shows the optical microscope image of UCL spot on the device with the laser excitation direction perpendicular to the grating orientation. The UCL spot on UCNP deposited QZAI PC is labeled A in Fig. 5(b) whereas the PL spot on the adjacent UCNP deposited plain grating (solid silicon slab as opposed to hole patterns in the QZAI) is labeled B. The PL intensity at A is much stronger than B, which confirms the higher intensity measurement is the result of NIR light self-confinement by QZAI PC.[5] Essentially, the QZAI PC confines and guides 1550 nm light whereas the 1D grating diffracts it. When rotating the laser excitation direction parallel to the 1D grating orientation [Fig. 5(c)], the light cannot be confined by the structure. The incident light is diffracted and therefore, the PL signal from the UCNPs (labeled C) is much weaker. Comparing the PL intensity of UCNPs deposited QZAI PC laser illuminated in x direction (spot A) and z direction (spot C), we find the PL intensity of A to be $\sim 4\times$ that of C [Fig. 5(d)].

In this setup, we were able to observe confinement of the NIR light with the UCNPs. In the future we will optimize illumination conditions to allow the observation of collimation and propagation ($\theta = 0°$) of NIR incident radiation using the nanoparticle-assisted UCL emission.

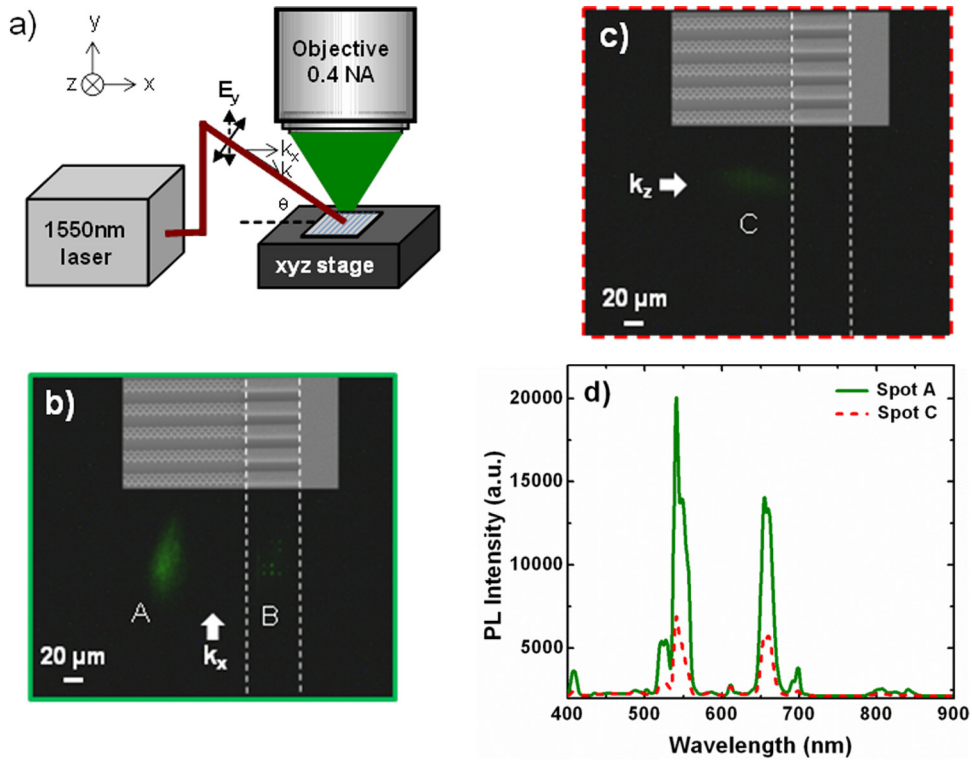

FIG. 5. (Color online) Measurement of PL signal from UCNP deposited structures (a) imaging setup and illumination axes; (b) CCD images of UCNP deposited QZAI PC (spot A) and UCNP deposited silicon grating (spot B) with laser excitation predominantly in the x direction and the laser is p-polarized. Confinement by the QZAI PC causes A to be brighter than B; (c) CCD image of UCNP deposited PC (Spot C) at laser excitation in the z direction with p-polarization; parallel to the surface; (d) PL spectrum of UCNP deposited PC for spots A and C at power density 500 W/cm^2. The intensity in the x direction (Spot A) is ~4 x that in the z direction (Spot C) due to confinement by the QZAI when illuminated perpendicular to the grating direction.

VI. CONCLUSIONS

Upconverting nanoparticles probes were exploited to detect the field enhancement in a QZAI photonic crystal structure under NIR excitation. The Er^{3+} doped β-NaYF4 nanoparticles in hexane were synthesized and dispersed uniformly by size. A deposition process was developed to ensure a thin film of UCNP uniformly deposited over the large area PC structure. The green light emitting UCNPs were used as a probe to detect NIR field confinement in the QZAI PC with conventional optical microscopy. Future microscopy setups will be optimized to observe light propagation in the QZAI PC using the UCNP probes.

ACKNOWLEDGMENTS

We acknowledge Bruce Harteneck and Erin Wood for support throughout. This work was performed at the Molecular Foundry Lawrence Berkeley National Laboratory, and was supported by the Office of Science, Office of Basic Energy Sciences, Scientific User Facilities Division, of the U.S. Department of Energy under Contract No. DE-AC02—05CH11231.

[1]S. John, Phys Rev. Lett. **58**, 2486 (1987).
[2]E. Yablonovitch, Phys Rev. Lett. **58**, 2059 (1987).
[3]D. R. Gamelin and H. U. Güdel, *Upconversion Processes in Transition Metal and Rare Earth Metal Systems* (Springer, Berlin, 2001).
[4]F. Auzel, Chem Rev. **104**, 139 (2004).
[5]V. Mocella, S. Cabrini, A. S. P. Chang, P. Dardano, L. Moretti, I. Rendina, D. Olynick, B. Harteneck, and S. Dhuey, Phys Rev. Lett. **102**, 133902 (2009).
[6]R. Chatterjee, N. C. Panoiu, K. Liu, Z. Dios, M. B. Yu, M. T. Doan, L. J. Kaufman, R. M. Osgood, and C.W. Wong, Phys Rev. Lett. **100**, 187401 (2008).
[7]P. S. Golding, S. D. Jackson, T. A. King, and M. Pollnau, Phys Rev. B **62**, 856 (2000).
[8]M. P. Hasselbeck, E. W. Van Stryland, and M. Sheik-Bahae, J. Opt. Soc. Am. B **14**, 1616 (1997).
[9]G. Chen, T. Y. Ohulchanskyy, A. Kachynski, H. Ågren, and P. N. Prasad, ACS Nano **5**, 4981 (2011).
[10]M. W. Pruessner, W. S. Rabinovich, T. H. Stievater, D. Park and J. W. Baldwin, J. Vac. Sci. Technol. B **25**, 21 (2007).
[11]Y. Wu, D. L. Olynick, A. Goodyear, C. Peroz, S. Dhuey, X. Liang, S. Cabrini, Microelectron. Eng. **88**, 2785 (2011).
[12]A. F. Isakovic, K. Evans-Lutterodt, D. Elliott, A. Stein, and J. B. Warren, J. Vac. Sci. Technol. A **26**, 1182 (2008).
[13]R. Dussart, M. Boufnichel, G. Marcos, P. Lefaucheux, A. Basillais, R. Benoit, T. Tillocher, X. Mellhaoui, H. Estrade-Szwarckopf, and P. Ranson, J. Micromech. Microeng. **14**, 190 (2004).
[14]M. de Boer, J. G. E. H. Gardeniers, H. V. Jansen, E. Smulders, M. J. Gilde, G. Roelofs, J. N. Sasserath and M. Elwenspoek, J. Microelectromech. Syst. **11**, 385 (2002).
[15]H. S. Qian and Y. Zhang, Langmuir, **24**, 12123 (2008).
[16]C.-J. Carling, F. Nourmohammadian, J.-C. Boyer, N. R. Branda, Angew. Chem. Int. Ed. **49**, 3782 (2010).
[17]G. H. Dieke and H. M. Crosswhite, Appl. Opt. **2**, 675 (1963).
[18]J. J. Wang, L. Chen, S. Tai, X. Deng, P. F. Sciortino, J. Deng, and F. Liu, J. Lightw. Technol., **23**, 474 (2005).